drones

MDPI

Article

A Sparse Feature-Based Mixed Signal Frequencies Detecting for Unmanned Aerial Vehicle Communications

Yang Wang [1], Yongxin Feng [1,*], Fan Zhou [1], Xi Chen [2], Jian Wang [3] and Peiying Zhang [4]

[1] School of Information Science and Engineering, Shenyang Ligong University, Shenyang 110158, China; wangyang@sylu.edu.cn (Y.W.); zhoufan@sylu.edu.cn (F.Z.)
[2] State Key Laboratory of Space Network and Communications, Tsinghua University, Beijing 100084, China; chenxiee@tsinghua.edu.cn
[3] College of Science, China University of Petroleum (East China), Qingdao 266580, China; wangjiannl@upc.edu.cn
[4] College of Computer Science and Technology, China University of Petroleum (East China), Qingdao 266580, China; zhangpeiying@upc.edu.cn
* Correspondence: fengyongxin@sylu.edu.cn

Abstract: As drone technology develops rapidly and many users emerge in airspace networks, various forms of interference have caused the wireless spectrum to exhibit a dense, diverse, and dynamic trend. This increases the probability of spectrum conflicts among users and seriously impacts the quality and transmission rate of communication. How to effectively improve the detection accuracy of each frequency component in the electromagnetic space mixed signals and avoid spectrum conflicts will become one of the crucial issues currently faced by unmanned aerial vehicle (UAV) communication technologies. However, the existing methods overlook the mutual interference among the component signals as well as the noise during the frequency detection process, which affects their detection performance. In this paper, we propose a mixed-signal frequency detection method based on the reconstruction of sparse feature signals. Without information such as frequency range, bandwidth, and the number of components, it can utilize the autoencoder network to learn the sparse features of each component signal in the high-dimensional frequency domain space and construct a nonlinear reconstruction function to reconstruct each component signal in the mixed signal, thereby realizing the separation of signals. On this basis, complex dilated convolution and deconvolution are used successively to perform feature extraction on the separated signals, which enhances the receptive field and frequency resolution ability of the network for signals, reduces the interference between noise and different component signals, and realizes the accurate estimation of the number of components and carrier frequencies. The simulation results show that when $SNR \geq 6$ dB, the detection accuracy of the number of component signals is greater than 96.3%. The detection error and detection accuracy of component frequencies are less than 3.19% and greater than 90.7%, respectively.

Keywords: UAV communication; neural network; frequency estimation; signal detection

Academic Editor: Rosdiadee Nordin

Received: 2 December 2024
Revised: 26 December 2024
Accepted: 2 January 2025
Published: 6 January 2025

Citation: Wang, Y.; Feng, Y.; Zhou, F.; Chen, X.; Wang, J.; Zhang, P. A Sparse Feature-Based Mixed Signal Frequencies Detecting for Unmanned Aerial Vehicle Communications. *Drones* **2025**, *9*, 34. https://doi.org/10.3390/drones9010034

1. Introduction

The communication of unmanned aerial vehicles (UAVs) constitutes a crucial part of the UAV technology system. Possessing advantages like mobility, stability, and extensive coverage, they can act as an aerial base station or relay node to aid ground communication. As an important means of information gathering and data transmission, UAVs are widely applied in both military and civilian domains. As shown in Figure 1, UAVs, with their

unique advantages, can achieve long-distance wireless data transmission (remote sensing and remote control via satellite as an intermediary) in multiple scenarios (such as power inspection, disaster relief, etc.), promoting the process of information interaction and information collaboration. However, the emergence of a large number of users in the airspace network has promoted the continuous development of intensive applications. This, in turn, has led to mutual occupation and interference of communication frequencies, seriously impacting the communication quality of UAVs. Therefore, in the crowded electromagnetic spectrum space, improving the utilization rate of the electromagnetic space spectrum and reducing the probability of spectrum conflicts are of great significance for promoting the rapid development of UAV communication technology.

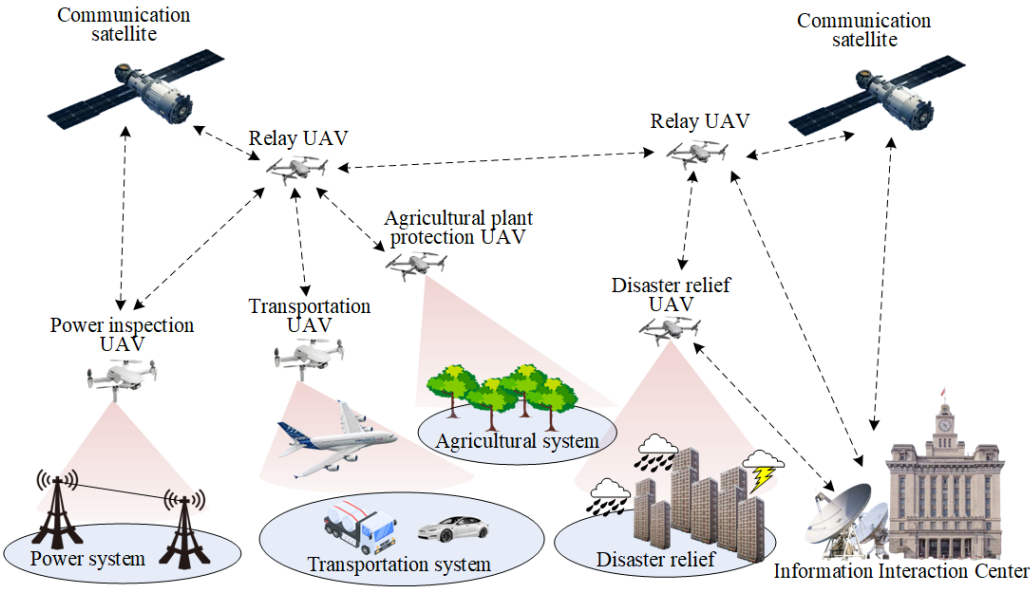

Figure 1. Schematic diagram of drone application scenarios.

Signal frequency detection is an important technology for real-time monitoring and analysis of the electromagnetic space spectrum. It provides reliable data support for the formulation of UAV communication strategies and electromagnetic spectrum management. The UAV communication system optimizes signal power and selects the best band based on the detected spectrum, avoiding strong interference bands to ensure stable and reliable communication. For example, if a strong electromagnetic interference is detected in a specific area within a certain frequency band, the UAV can dynamically switch to a relatively idle and less interfering frequency band for communication, thus ensuring the integrity and timeliness of data transmission. However, as the number of communication terminals increases, numerous factors such as the diversification of communication systems and the advancement of modulation waveforms have resulted in an increasingly complex electromagnetic environment, presenting a tremendous challenge to the detection of wireless signal frequencies [1,2].

In general, the electromagnetic space in which the UAV communication system operates is composed of a mixture and interweaving of signals with various frequencies and formats. In recent years, the detection of mixed signals and the estimation of each carrier frequency have received extensive attention. The commonly used methods mainly include: energy threshold detection method [3–7], wavelet perception method [8–13], and signal frequency detection method based on compressed sensing [14–19], and so on. The energy detection method achieves signal detection by accumulating energy in the time domain, frequency domain, or transform domain of the signal and then comparing it with a preset threshold value. This approach offers the advantages of ease of implementation and rela-

tively low computational complexity. However, this method has poor noise resistance and cannot meet the reliability requirements of UAV communication under strong interference conditions. The wavelet perception method employs continuous wavelet transform in the frequency domain to achieve the detection of frequency points in the spectrum. This approach has a high resolution for each subcarrier frequency and an excellent suppression effect on noise. Nevertheless, when the sampling frequency is low, it will result in a decrease in frequency resolution and impact the detection effect of subcarrier signals. The signal detection method based on compressed sensing realizes signal detection by utilizing the sparse characteristics of the signal spectrum. It effectively reduces the number of sampling points and saves the operating cost of the detection system. However, this method has a large amount of computation and high requirements for hardware, making it difficult to meet the low energy consumption requirements of unmanned aerial vehicles.

From this, it can be known that traditional detection methods are limited by factors such as noise, frequency resolution, and energy consumption, and can no longer meet the demand for signal detection capabilities of UAV communication [20,21]. In recent years, with the increasing maturity of deep neural network technology, remarkable results have been achieved in multiple fields. At the same time, it has also opened up a completely new way for the development of signal frequency detection technology.

Currently, the signal frequency detection method based on neural networks is in the developmental stage. Some scholars have conducted relevant research in this area. In [22,23], the authors proposed a spectrum sensing method based on deep neural networks. By capturing the temporal correlation characteristics of the target signal, it realizes effective detection of signal frequency under low signal-to-noise ratio. To enhance the universality and adaptability of the frequency detection system under complex noise models, in [24,25], a universal noise model is constructed, and the design of the objective loss function is optimized according to the noise distribution function. However, the aforementioned methods merely take into account the determination of whether there is a signal within a specific frequency band, while neglecting the accurate estimation of the signal frequency value. In response to this issue, Izacard G. and others put forward a signal detection and frequency estimation method based on high-resolution spectral line representation of deep neural networks [26]. This approach employs neural networks to achieve high-resolution representation of the spectrum of the mixed signal and realizes the estimation of the frequency of each component by means of the peak search method. Compared with traditional methods, it has a higher estimation accuracy. However, since the peak search method requires prior information such as the number of frequency components, it limits the application scope of this method. Reference [27] proposed a data-driven frequency estimation method for mixed signals. Building on the method in [26], by adding a component number estimation network, this approach accomplishes the detection of the number of sub-signals in the mixed signal, averts relying on prior information, and enhances the universality of the method.

Pan [28] et al. achieved the detection of two-dimensional frequency signals through the reconstruction of spectral lines, further improving the accuracy of signal frequency estimation. Signal detection methods relying on the idea of high-resolution representation of spectral lines can effectively estimate the frequency of low-resolution mixed signals. However, since it requires continuous upsampling of data to improve the resolution ability of the method, it leads to excessive computational complexity and a large number of parameters, reducing the performance of the method. A signal frequency detection method based on the theory of continuous signal reconstruction and noise interference elimination is proposed in the [29]. Under the premise of low amounts of parametric and computational, this method accomplishes the detection and frequency estimation of low-resolution mixed

signals. However, due to noise and the existence of mutual interference among sub-signals, it leads to the degradation of the detection performance of the method for mixed signals and affects the accuracy of the frequency estimation of sub-signals. In [30], a neural network signal frequency detection method based on the signal adaptive modal decomposition theory is proposed. According to the modal decomposition theory, a fully connected neural network is constructed to realize the separation of signal and noise, effectively improving the anti-noise ability of the method. However, there is still mutual interference between sub-signals.

In a complex electromagnetic environment, mixed-signal components interfere. Frequency resolution drops. Existing neural network-based methods for frequency detection and estimation can't meet UAV communication needs for reliability and effectiveness. Inspired by the concepts of feature sparse representation and signal separation as mentioned in [31–34], this paper presents a mixed-signal frequency detection method, SFsRNet, based on sparse feature signal reconstruction. This approach achieves the separation of each component signal by learning the sparse features and reconstruction function of the mixed signal. On this foundation, it realizes the detection of the number of components in the mixed signal and the estimation of frequency, and then verifies and evaluates its performance.

The major contributions of this work can be summarized as follows:

1. The SFsRNet method is proposed. Under the conditions of low signal-to-noise ratio and low frequency resolution, it realizes the detection of the frequency of each component of the mixed signal, providing a guarantee for the reliable communication of UAV.

2. The proposed SFsRNet method extracts the sparse features of each component signal in the mixed signal and constructs a nonlinear reconstruction function to achieve the separation of each component signal, thereby avoiding the mutual interference between component signals during parameter estimation.

2. Mechanism of Mixed-Signal Separation Detection Method

The expression for the mixed signal $Y(t)$ received in the electromagnetic space is shown in Equation (1).

$$Y(t) = \sum_{i=1}^{m} X_i(t) + N(t) \tag{1}$$

where $Y(t)$ contains m component signals and noise $N(t)$, the number of components $m \geqslant 1$, and $X_i(t)$ represents the i-th component signal. The error between $X_i(t)$ and $\hat{X}_i(t)$ is given in Equation (2).

$$error_i = E||X_i(t) - \hat{X}_i(t)||_2^2 \tag{2}$$

where $\hat{X}_i(t)$ is the estimated value of $X_i(t)$.

As indicated in [35], signals have sparsity in the frequency domain. By utilizing this characteristic, signal reconstruction can be achieved by constructing a nonlinear mapping function. The reconstruction process is shown in Equation (3).

$$\hat{X}_i(t) = DTFT^{-1}(M_i(f)Y(f)) \tag{3}$$

where $Y(f)$ and $\hat{X}_i(f)$ are representations of $Y(t)$ and $\hat{X}_i(t)$ in the frequency domain, respectively. $DTFT^{-1}$ is the inverse discrete Fourier transform, $M_i(f)$ is a nonlinear function constructed based on the sparse feature $\hat{Y}(f)$ of $Y(f)$, which is used to map $Y(f)$ to $\hat{X}_i(f)$. From the Equations (2) and (3), by minimizing $error_i$, the optimization of $\hat{Y}(f)$ and $M_i(f)$ is achieved, and then the separation of the signal and the estimation of frequencies are completed.

Deep neural network technology can extract the sparse features of the input signal and construct a nonlinear mapping function according to the target optimization function,

thereby completing the separation of the mixed signals. In this paper, the signal separation objective optimization function is shown in Equation (4).

$$\begin{aligned} Loss_c = \sum_{i=1}^{M} MSE(X_i(t) - \underbrace{\left(DTFT^{-1}(CSnet(\omega_c, Y(t))Y(f)\right)}_{\hat{X}_i(t)} \\ + MSE(N(t) - \underbrace{DTFT^{-1}(CSnet(\omega_c, Y(t))Y(f)))}_{\hat{N}(t)} \end{aligned} \tag{4}$$

where $MSE(\cdot)$ is the minimum mean square error operation, M represents the maximum number of separable components for the network. $CSnet(\cdot)$ denotes the signal separation network for extracting sparse features in the frequency domain of the signal and constructing the nonlinear reconstruction function, and ω_c is the weight parameter of $CSnet(\cdot)$. The network optimizes and adjusts the parameter so that the true components and noise in the mixed signal are close to the estimated values. That is, when $Loss_c$ converges, the optimal weight ω_c^* of the network is obtained, thereby realizing the separation of the mixed signal. The specific calculation process is as shown in Equations (5) and (6).

$$\omega_c^* = \underset{\omega_c}{argmin}(Loss_c) \tag{5}$$

$$\hat{X}_1(t), \ldots, \hat{X}_M(t), \hat{N}(t) = DTFT^{-1}(CSnet(\omega_c^*, Y(t))Y(f)) \tag{6}$$

In Equation (6), $\hat{X}_1(t) \ldots, \hat{X}_M(t)$ are the estimated values of each component of the mixed signal. $\hat{N}(t)$ is the estimated value of the noise

A component number detection network is constructed to achieve the estimation of m. The objective optimization function of this network is shown in Equation (7).

$$Loss_m = MSE\left(m - DMnet\left(\omega_m, \textstyle\sum_{i=1}^{M} \hat{X}_i(t)\right)\right) \tag{7}$$

In Equation (7), $DMnet(\cdot)$ is the component number detection network; ω_m is the weight parameter of $DMnet(\cdot)$. This network takes the separated component signal $\hat{X}_i(t)$ in the mixed signal as input. By minimizing $Loss_m$, it optimizes the parameter, eliminates the erroneously separated signal components, and makes the estimated value $\hat{m}$ close to the true component number m . The specific calculation process is shown in Equations (8) and (9).

$$\omega_m^* = \underset{\omega_m}{argmin}(Loss_m) \tag{8}$$

$$\hat{m} = DMnet\left(\omega_m^*, \textstyle\sum_{i=1}^{M} X_i(t)\right) \tag{9}$$

For $\hat{X}_1(t) \ldots, \hat{X}_M(t)$ separated in Equation (6), a frequency estimation network is constructed to achieve the estimation of f_i . The objective optimization function of this network is shown in Equation (10).

$$Loss_g = \textstyle\sum_{i=1}^{M} MSE\left(f_i - Gnet\left(\omega_g, \hat{X}_i(t), \hat{m}\right)\right) \tag{10}$$

where $Gnet(\cdot)$ is the parameter estimation network, ω_g is the weight parameter of the $Gnet(\cdot)$, and $Gnet(\cdot)$ takes $\hat{X}_i(t)$ and $\hat{m}$ as inputs to estimate the estimated value of each component frequency $\hat{f}_i$ in the mixed signal. The optimal weight parameter ω_g^* of the network is obtained by minimizing the $Loss_g$, and then the accurate estimation of the

realized frequency is gained. The computational procedure is shown in Equations (11) and (12).

$$\omega_g^* = \underset{\omega_g}{argmin}\left(Loss_g\right) \tag{11}$$

$$\hat{f}_i = \mathrm{Gnet}\left(\omega_g^*, \hat{X}_i(t), \hat{m}\right) \quad i = 1, 2, \ldots, M \tag{12}$$

As shown in Figure 2, the overall flow of the frequency detection method is based on sparse feature signal reconstruction. This process is composed of two parts: signal separation and component number and frequency estimation. In the signal separation process, for the mixed signal $Y(t)$, Fourier transform and sparse feature extraction are performed in sequence. According to the sparse feature $\hat{Y}(t)$, the nonlinear mapping relationship $M_i(f)$ from $Y(t)$ to $\hat{X}_i(f)$ is constructed to achieve signal separation. During the process of component number and frequency estimation, feature extraction is performed on each component signal in the mixed signal, respectively. Eventually, the estimation of the number and frequency of component signals is completed.

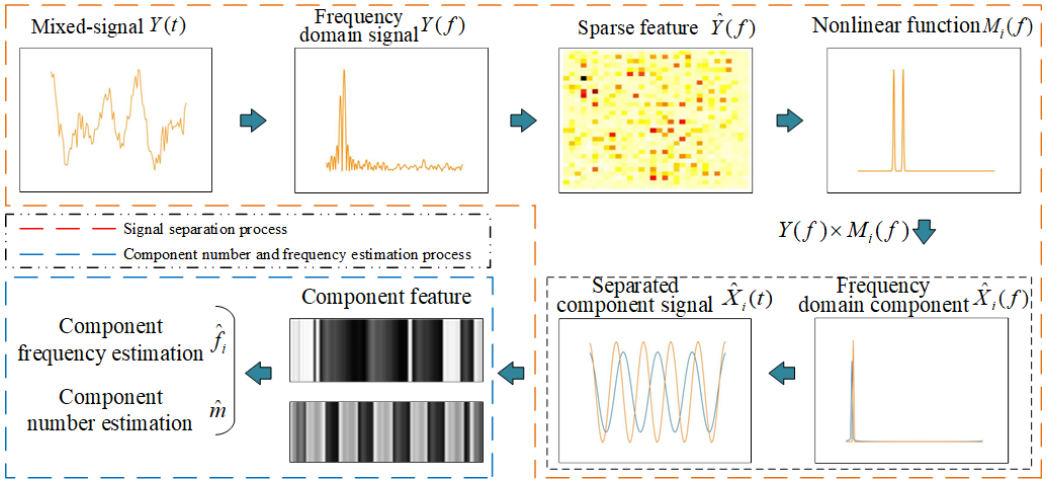

Figure 2. Frequency detection flow based on sparse feature signal reconstruction.

3. Mixed-Signal Separation Frequency Detection Network Framework

The frequency detection network framework based on sparse feature signal reconstruction is composed of three parts: signal separation network, component number detection network, and component frequency detection network.

The signal separation network uses the autoencoder network as its backbone. The encoder extracts the sparse features of each component signal in the mixed signal. The decoder then constructs a nonlinear mapping function based on these sparse features to separate each component signal. As shown in Figure 3, the network design is as follows. The signal separation network transforms the mixed signal $Y(t)$ to the frequency domain through two fully connected layers, and its frequency domain representation is $Y(f)$. Then, multiple convolutional layers and pooling layers are cascaded to construct the encoder and perform downsampling processing on $Y(f)$ to obtain the sparse feature $\hat{Y}(f)$ of $Y(f)$. The decoder is composed of multiple convolutional layers and deconvolutional layers. It performs upsampling and reconstruction on $\hat{Y}(f)$. Through the Spatial Group-wise Enhance (SGE) module [36], the features of each component signal are grouped. The similarity between local and global features is utilized to generate an attention mask for realizing the construction of the nonlinear reconstruction function $M_i(f)$ in the frequency domain of each component signal.

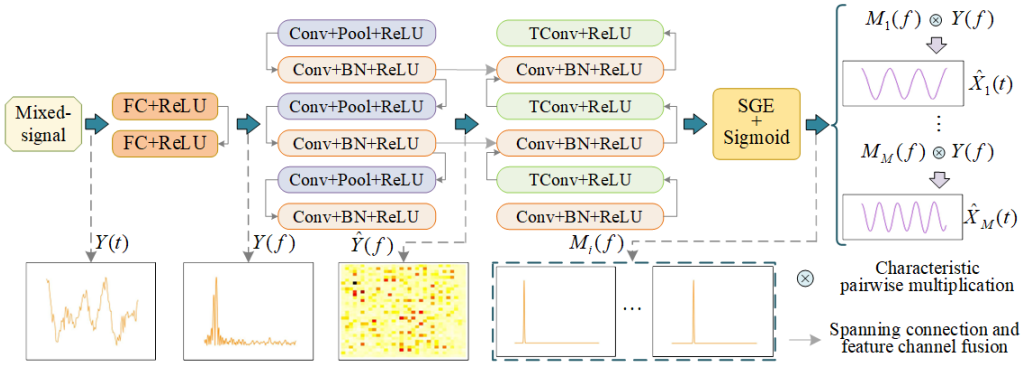

Figure 3. Signal separation network structure design.

In addition, this network uses skip connections to fuse shallow features and deep features by channels, enhancing the network's ability to construct the nonlinear mapping function $M_i(f)$. Meanwhile, multiple BN layers and activation layers are employed to increase the convergence speed of network training [37]. Taking the case where the maximum estimated number of component signals by the network $M \leqslant 5$ as an example, Table 1 presents the parameters of the signal separation network.

Table 1. Signal separation network parameters.

Layer Name	Number of Filters/Neurons	Kernel Size	Output Dimension
FC+ReLU	100	-	1×1024
FC+ReLU	1024	-	1×1024
Conv+Pool+ReLU	16	$3 \times 3/2 \times 2$	16×16
Conv+BN+ReLU	16	3×3	16×16
Conv+Pool+ReLU	32	$3 \times 3/2 \times 2$	8×8
Conv+BN+ReLU	32	3×3	8×8
Conv+Pool+ReLU	64	$3 \times 3/2 \times 2$	4×4
Conv+BN+ReLU	64	3×3	4×4
Conv+BN+ReLU	64	3×3	4×4
TConv+ReLU	32	2×2	8×8
Conv+BN+ReLU	32	3×3	8×8
TConv+ReLU	16	2×2	16×16
Conv+BN+ReLU	16	3×3	16×16
TConv+ReLU	6	2×2	32×32
SGE+Sigmoid	6	1×1	32×32

In Table 1, the output data of the SGE+Sigmoid layer has a dimension of 32×32 and a channel number of 6. According to the channel number, it is divided into six parts. Five of these parts are sub-signal frequency domain masks, and the remaining part is the noise frequency domain mask, which is the nonlinear reconstruction mapping function $\hat{M}_i(f)$. Multiplying $M_i(f)$ by $Y(f)$ yields the frequency domain estimated value $\hat{X}_i(f)$ of the component signal. Ultimately, the separation of each sub-signal and noise is achieved.

The component number detection network is employed to accomplish the estimation of the number of components in the mixed signal and offer data support for the accurate detection of signal frequencies. The design of its network structure is illustrated in Figure 4. The network composed of three convolutional layers, one deconvolutional layer, and two fully connected layers. The channel fusion of $\hat{X}_1(t), \ldots, \hat{X}_M(t)$ is used as the input to the network. The first convolutional layer employs 2×3 convolutional kernels to obtain the correlation features of the in-phase and quadrature components of the time-domain signal, effectively reducing the amount of computation in the network. The second and third convolutional layers perform up-channel processing to obtain the correlation features of the

time-domain signal in a high-dimensional space. At the same time, a convolutional stride of 1×2 is adopted to limit the overhead of the network. The deconvolution layer fuses the data features of multiple channels. Then, two fully connected layers and SoftMax are used to estimate the probabilities $P_1, \ldots, P_M$ of the number of components. Finally, the estimated value of the number of components in the mixed signal is obtained. The main parameters of this network are shown in Table 2.

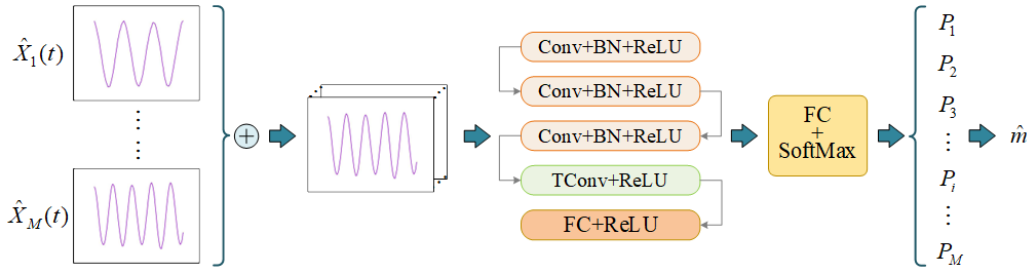

Figure 4. Component number detection network structure design.

Table 2. Parameters of component number detection network.

Layer Name	Number of Filters/Neurons	Kernel Size	Output Dimension
Conv+BN+ReLU	16	2×3	1×100
Conv+BN+ReLU	32	1×3	1×50
Conv+BN+ReLU	64	1×3	1×25
TConv+ReLU	1	1×5	1×125
FC+ReLU	125	-	32
FC+SoftMax	32	-	5

The component frequency detection network constructs M frequency detection modules to estimate the frequencies of $\hat{X}_1(t), \ldots, \hat{X}_M(t)$ respectively. According to the number of components, the output results of the first $\hat{m}$ frequency detection modules are taken as the estimated values of the frequencies of each component signal in the mixed signal. The structural design of the component frequency detection network is shown in Figure 5. The frequency detection module is composed of three complex dilated convolutional layers, one deconvolutional layer, and two fully connected layers. The complex dilated convolutional layer independently extracts the features of the in-phase and quadrature components of the time-domain signal, thereby enhancing the diversity of feature extraction and expanding the receptive field of the data. The dilation rates of the three complex dilated convolutional layers are set to 1, 2, and 5 in sequence to prevent information loss resulting from the grid effect. The deconvolution layer conducts 5 times upsampling on the input features, which augments the module's frequency discrimination capability and raises the accuracy of frequency detection for each component. Lastly, two fully connected layers are employed to establish the mapping relationship between features and frequencies, thus achieving the estimation of the frequencies of component signals. As shown in Table 3, the main parameters of the frequency detection module are presented. In this paper, it is assumed that the number of components in the mixed signal is no more than 5. Consequently, the output dimension of the FC+Tanh layer is 5. In practical applications, the parameters can be adjusted finely according to specific needs.

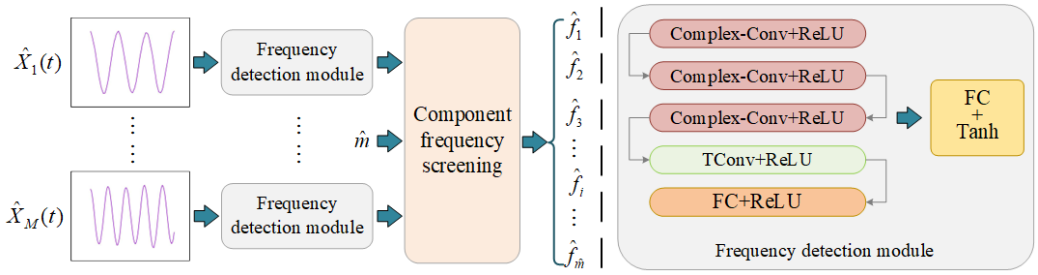

Figure 5. Component frequency detection network structure design.

Table 3. Parameters of the component signal frequency detection network.

Layer Name	Number of Filters/Neurons	Kernel Size	Output Dimension
Complex+Conv+ReLU	36	3×3	2×100
Complex+Conv+ReLU	36	1×3	2×100
Complex+Conv+ReLU	36	1×3	1×25
TConv+ReLU	1	2×5	1×500
FC+ReLU	500	-	64
FC+Tanh	64	-	5

Algorithm 1 presents the design of the training and inference methods for the mixed-signal separation frequency detection network framework. This approach sequentially trains the signal separation network, the component signal number detection network, and the sub-component signal frequency detection network. The weights are optimized and updated according to the loss functions of each network. Based on the optimized networks, the detection of component number and frequency in the mixed signal is achieved.

Under extreme conditions, the features extracted by SFsRNet will have outliers, which will have a negative impact on the estimation results of the mixed-signal frequencies. To enhance the robustness of the method proposed in this paper under abnormal conditions, replace $MSE(\cdot)$ in Equations (4), (10), and (11) with $Huber(\cdot)$. *Huber* is a loss function with relatively strong robustness, which combines the advantages of mean squared error and absolute error, respectively. It can maintain a smooth quadratic loss when the error is small and can also avoid the influence of large errors on the model. Equation (13) presents the expression of the Huber loss function.

$$L_\delta(\alpha) = \begin{cases} \frac{1}{2}\alpha^2 & |\alpha| \le \delta \\ \delta\left(|\alpha| - \frac{1}{2}\delta\right) & |\alpha| > \delta \end{cases} \tag{13}$$

where α represents the difference between the estimated value and the true value. δ is a hyperparameter that is used to control the threshold of the error magnitude calculation method. When $\delta > |\alpha|$, $L_\delta(\alpha)$ is identical to the mean squared error loss function and has the properties of smoothness and continuity, which makes it suitable for situations where the error is small. When $\delta \le |\alpha|$, $L_\delta(\alpha)$ is the same as the absolute error loss, thus avoiding the squaring operation in the case of large errors and reducing the excessive influence of outliers on the model training.

Algorithm 1 Network framework training and inference methods.

Method Name: Training and Inference of Mixed-Signal Separation Frequency Detection Network Framework.
Training inputs: input data /*Mixed-signal, obtained from Equation (1)*/
Training outputs: *CSnet* /*Signal separation network model*/, *DMnet* /*Component number detection network model*/, *Gnet* /*Component frequency estimation network model*/
1: Divide $Y(t)$ into n parts, with each part consisting of m samples. The ith part of the samples is denoted as $y_i(t)$.
2: for $epoch \leftarrow 1 : N$/* "$epoch$" refers to the number of training rounds. "N" represents the overall number of training rounds*/
3: while $lr < lr_\lambda$/*"lr" stands for the learning rate. "lr_λ" denotes the threshold value of the learning rate. Training is stopped when $lr < lr_\lambda$ */
4: for $i \leftarrow 1 : n$
$\hat{X}_1(t), \ldots, \hat{X}_M(t), \hat{N}(t) \leftarrow DTFT^{-1}(\text{CSnet}(\omega_c, y_i(f))y_i(f))$
/*The error value $Loss_c$ is obtained according to Equation (4), and the weight ω_c of *CSnet* is optimized by using Equation (5) */
$\hat{m} \leftarrow DMnet\left(\omega_m, \sum_{i=1}^{M} \hat{X}_i(t)\right)$ /*The error value $Loss_m$ is obtained according to Equation (7), and the weight ω_m of *CSnet* is optimized by using Equation (8)*/
$\hat{f} \leftarrow Gnet(\omega_g^*, \hat{X}_k(t), \hat{m}) k \leftarrow 1, 2, \ldots, M$ /* The error value $Loss_g$ is obtained according to Equation (10), and the weight ω_g of *Gnet* is optimized by using Equation (11) */
$Loss \leftarrow Loss_c + Loss_g + Loss_m$
5: end for
6: end while
7: When *Loss* does not descend for 5 consecutive rounds $lr \leftarrow 0.8 * lr$ /*$Loss$ is the total error value*/
8: end for
Inference input: $Y_{test}(t)$ /* The mixed-signal is obtained by Equation (1) and is completely different from $Y(t)$ */
Inference output: $\hat{f}_k \; k \leftarrow 1, 2, \ldots, m$
1: $\hat{X}_1(t), \ldots, \hat{X}_M(t), \hat{N}(t) \leftarrow DTFT^{-1}(\text{CSnet}(\omega_c^*, Y_{\text{test}}(t)Y_{\text{test}}(f))$
/*ω_c^* is the optimized weight value of the signal separation network */
2: $\hat{m} \leftarrow \text{DMnet}\left(\omega_m^*, \sum_{i=1}^{M} \hat{X}_i(t)\right)$ /*ω_m^* is the optimized weight value of the sub-signal number detection network */
3: $\hat{f} \leftarrow Gnet(\omega_g^*, \hat{X}_k(t), \hat{m}) \; k \leftarrow 1, 2, \ldots, M$ /* ω_g^* is the optimized weight value of the sub-signal frequency detection network, When $k > \hat{m}$, $\hat{f}_k \leftarrow 0$ */
4: Return $\hat{f}_k$,$\hat{m}$

4. Simulation Verification and Analysis

4.1. Dataset

To accurately verify the performance of the method proposed in this paper, the methods in references [27,36] are adopted to construct the training and validation datasets. The detailed generation method of the datasets is shown in Algorithm 2.

As indicated in [27], when the frequency interval between component signals is less than $1/N$, accurate detection of the frequencies of each component signal cannot be realized. When the frequency interval is between $1/N$ and $2/N$, detecting the frequencies of the individual component signals becomes highly challenging. Therefore, in this paper, the minimum frequency interval between each component signal is $1/N$, and the random interval follows a normal distribution with a mean of $\mu = 0$ and a variance of $\delta_2 = 0.25$.

Algorithm 2 Training set and validation set generation methods.

Method Name: Generation method of training set and validation set.

1: $m \in [1, \ldots, M]$/* Randomly select an integer from $[1, \ldots, M]$ to represent the number of components in the maxed-signal*/
2: $f_o \sim U(0, 0.25)$/* "f_0" represents the initial frequency of the component signal and obeys a uniform distribution */
3: $for\ i \leftarrow 1 : m$
$\omega_i \sim |N(0, 2.5/N)|$/* "$\omega_i$" represents the random interval of the frequency of each component signal and follows a normal distribution. N denotes the number of sample points*/
$f_i \leftarrow f_0 + i/N + \omega_i$/* "$f_i$" represents the frequency of the i th component signal */
$a_i \sim U(0.1, 1.0)$/* "a_i" represents the amplitude of the i th component signal */
$\varphi_i \sim U(0, 2\pi)$/* "$\varphi_i$" represents the phase of the i th component signal*/
4: end for
5: $Y \leftarrow \sum_{I=1}^{m} a_i epx(2\Pi j f_i n + \varphi_i) + N(n)$

As shown in Table 4, the main parameters of the training set and validation set are as follows. The total number of the training set is 80,000. The signal-to-noise ratio (SNR) ranges from −10 dB to 20 dB at an interval of 2 dB. For each SNR, there are 5000 training samples. The total number of samples in Validation Set 1 is 24,000. There are 1500 samples included under each SNR, and the number of components in each sample is randomly selected within $m \leq 5$. Validation set 2 has the same parameters as validation set 1. The difference is that the number of components of all samples is selected under the condition of $m = 1, 2 \ldots, 5$, and the number of samples under each number of components is 4800.

Table 4. Main parameters of training set and validation set.

Dataset	Total Number of Samples	SNR (dB)	Data Dimensions
training set	8 W	−10~20	2 × 100
validation set 1	2.4 W	−10~20	2 × 100
validation set 2	2.4 W	−10~20	2 × 100

4.2. Simulation Parameters and Evaluation Indicators

In this paper, the simulation is verified under the conditions of RTX3090 GPU and Python 3.9. The specific simulation parameters are shown in Table 5. In this setup, early stopping is applied when the loss does not decrease for 5 consecutive epochs, at which point the learning rate is reduced to 80% of its previous value. Training is stopped when the learning rate falls below 1×10^{-5}.

Table 5. Network training parameters.

Optimizer	Learning Rate	Epochs	Batch	Early Stopping
Adam	0.001	200	1024	Yes

Regarding the performance of the method proposed in this paper, it is evaluated and verified from two aspects: the detection accuracy rate of the number of components and the detection accuracy rate of component frequencies. The calculation methods are as shown in Equations (14)–(16).

$$\mathrm{Acc_m} = \frac{\mathrm{Sample_m}}{\mathrm{total}} \times 100\% \tag{14}$$

$$\mathrm{Acc_f} = \frac{\mathrm{Sample}_{(|f-\hat{f}|<\varepsilon)}}{\mathrm{total}} \times 100\% \tag{15}$$

$$\text{Error}_f = \frac{\sum_{total} \sum_{i=1}^{m} |f_i - \hat{f}_i|}{\sum_{total} \sum_{i=1}^{m} |f_i|} \times 100\% \tag{16}$$

Equation (14) represents the detection accuracy rate of the number of components. It is the total number of verification samples, and $sample_m$ represents the number of samples with the correct estimated number of components.

Equation (15) represents the detection accuracy rate of component frequencies. $f := (f_1, \ldots, f_m)$ is the true frequency value of the components in the mixed signal, and $\hat{f}$ is the estimated value of f. $\text{Sample}_{(|f-\hat{f}|<\varepsilon)}$ represents the number of samples with an estimated deviation value lower than the error threshold ε. It is worth noting that the number of sampling points N of the samples in this paper is 100, and the minimum frequency interval between each component in the mixed signal is 0.01. Therefore, ε is set to 0.01 and 0.02, respectively, to verify the frequency detection performance of SFsRNet.

Equation (16) represents the detection error of component frequencies. It is obtained by taking the ratio of the sum of the errors between the true values and estimated values of all components in the sample to the sum of the true frequency values of the components in the sample. Here, m is the number of component signals in a single sample.

4.3. Simulation Results and Analysis

In this section, firstly, validation set 2 is used to verify the signal separation performance of the SFsRNet method. Then, under the same experimental environment, using validation set 1 and validation set 2, from the two perspectives of detection accuracy rate of the number of components and detection accuracy rate of frequencies, a comparative verification is conducted with DeepNet [27], ResFreq-Net [28], SignalNet [29], SamdNet [30], and DnCNN-GRU [38].

Figure 6 presents the separation error of the SFsRNet method for the mixed signal under different numbers of components. It can be clearly observed from the figure that, except in the low signal-to-noise ratio (SNR) region where the influence of noise energy is relatively significant, resulting in a few minor fluctuations in the error values, on the whole, the error values show a decreasing trend as the SNR increases. When $SNR = 0$ dB, the error value is less than 0.0057. When $SNR = 10$ dB, the error value is less than 0.0012. When $SNR \geq 0$ dB and $m > 3$, the signal separation error values are relatively close. This indicates that the SFsRNet method is less influenced by the number of components under this condition and has a relatively stable separation effect.

Figure 7 presents a comparison between the component signals after the separation of the mixed signal and the original signals when $SNR = 0$ dB and 10 dB and $m = 4$. Among them, figures (a) to (d) respectively present the separation effects of each component signal in the same mixed signal. The blue line represents the original signal, and the yellow and red lines respectively represent the component signals after separation by 0 dB and 10 dB. As can be seen from the figure, when the SNR is 0 dB, the frequency of the separated signal is basically the same as that of the original signal, but there is a certain deviation in amplitude. When the SNR is 10 dB, the separated signal almost coincides with the original signal. Thus, it can be known that SFsRNet can effectively achieve signal separation and retain the frequency information of the original signal.

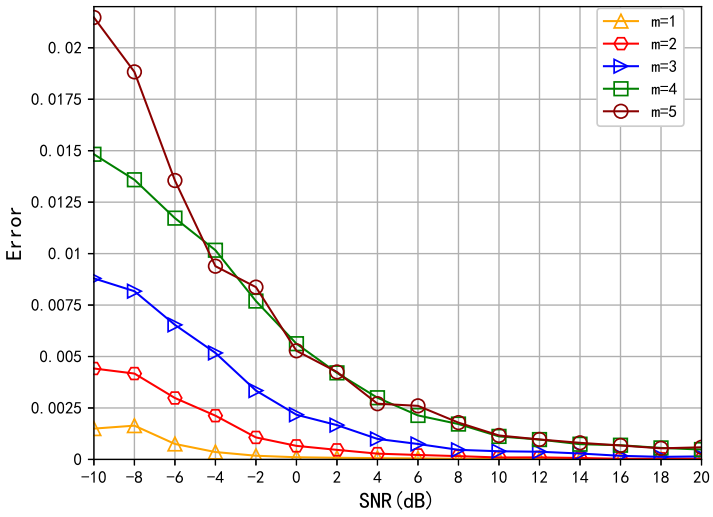

Figure 6. Signal separation error of SFsRNet method.

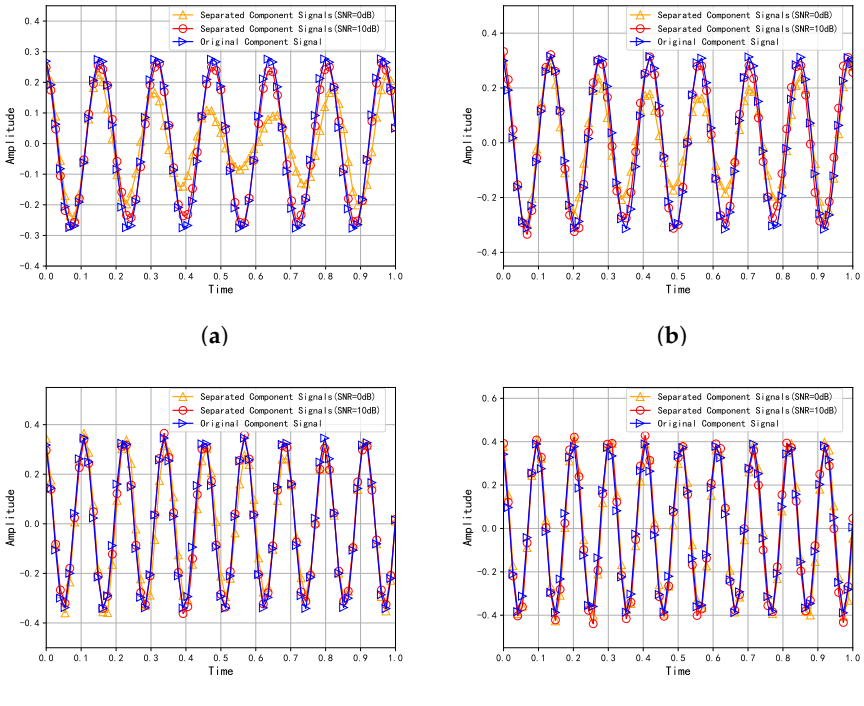

Figure 7. Comparison of the Time Domain Characteristics Between Separated and Original Sub-Signals. Panels (**a**–**d**) illustrate the separation results of individual component signals from the mixed-signal. Each component signal exhibits distinct amplitude, phase, and frequency characteristics. The blue right triangle denotes the original signal, while the yellow upward triangle and the red circle represent the separation results under signal-to-noise ratios (SNR) of 0 dB and 10 dB, respectively.

Figure 8 shows the comparison of the detection accuracy rates of the number of components in the mixed signal by the above six methods using validation set 1 under the condition of -10 dB $\leq SNR \leq$ 20 dB. As can be seen from the figure, the detection accuracy rate of SFsRNet is better than that of the other four methods under each SNR. When $SNR = -4$ dB, the detection accuracy rate of SFsRNet is 80.75%, exceeding the detection accuracy rates of other methods by 1.3% to 4.25%. When $SNR = 12$ dB, the detection accuracy rate of SFsRNet is 98.4%, which is 1.7% to 2.1% higher than that of other

methods. From this, it can be observed that the detection accuracy rate of SFsRNet for the number of components steadily increases as the SNR rises, indicating that this method possesses relatively good estimation ability for the number of components in mixed signals.

Table 6 showcases the detection accuracy rates of the aforementioned six networks utilizing validation set 2 under the condition where -10 dB $\leq SNR \leq 20$ dB for different quantities of components. As is evident from the table, SFsRNet exhibits a higher average detection accuracy rate compared to the other five methods across different numbers of components, thereby demonstrating that the method proposed in this paper possesses remarkable versatility in detecting the number of components.

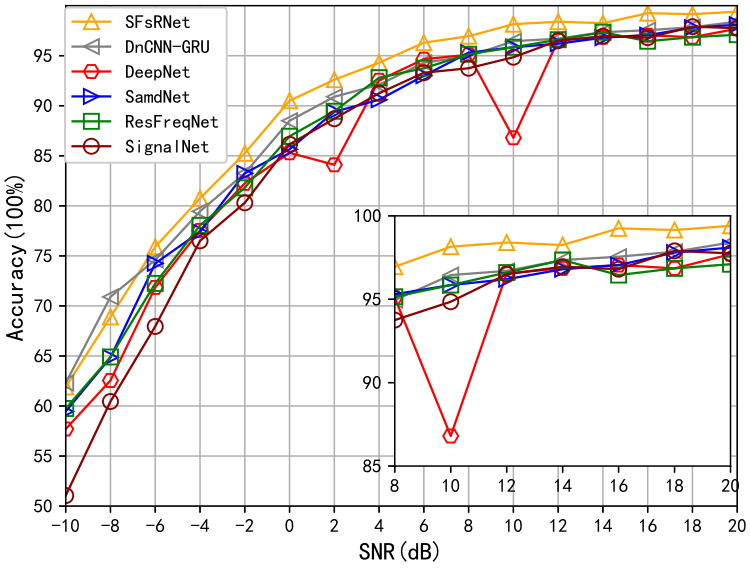

Figure 8. Comparison of component number detection accuracy.

Table 6. Mean detection accuracy for varying numbers of Components.

Method Name	m = 2	m = 3	m = 4	m = 5
DeepNet	86.96%	81.92%	79.33%	87.99%
ResFreqNet	89.98%	83.85%	80.07%	86.9%
SignalNet	88.46%	81.03%	73.93%	88.19%
SamdNet	88.83%	82.5%	77.22%	87.7%
DnCNN-GRU	90.12%	84.09%	80.23%	88.51%
SFsRNet	**90.88%**	**85.63%**	**82.51%**	**90.3%**

Figure 9 presents the detection errors of the frequencies of each component in the mixed signal by the above six methods under validation set 1. As can be directly observed from the figure, when -10 dB $\leq SNR \leq 20$ dB, the detection error of the component frequencies by SFsRNet is lower than that of other methods.

Table 7 presents the detection errors of component frequencies for the above six methods when $SNR = 0$ dB, $SNR = 10$ dB, and $SNR = 20$ dB. As can be seen from table, the detection errors of SFsRNet are respectively 0.81% to 14.59%, 1.4% to 14.55%, and 2.5% to 15.17% lower than those of the other five methods. From this, it can be known that as the signal-to-noise ratio increases, the detection error of the proposed method for frequency will gradually decrease, and its superiority becomes more and more obvious.

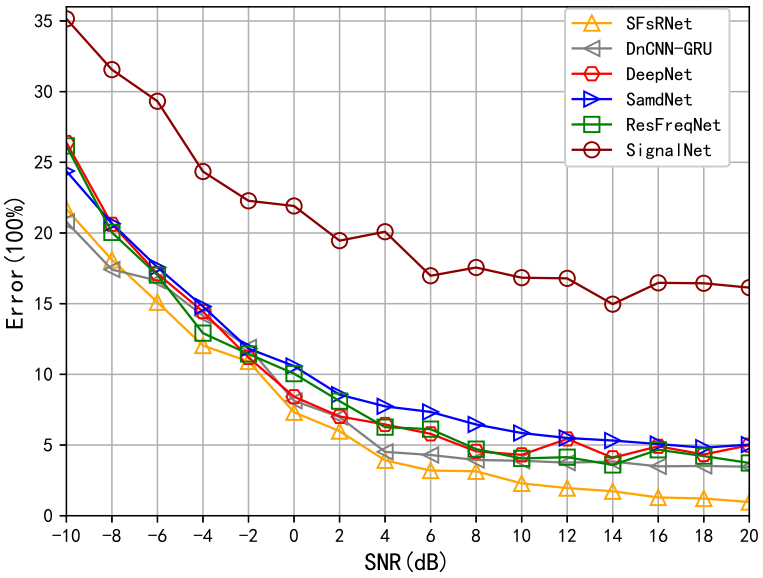

Figure 9. Comparison of component frequency detection error.

Table 7. Component Frequency Detection Errors.

Method Name	SNR = 0 dB	SNR = 10 dB	SNR = 20 dB
DeepNet	8.42%	4.31%	4.99%
ResFreqNet	10.05%	4.05%	3.73%
SignalNet	21.91%	16.83%	16.13%
SamdNet	10.59%	5.84%	5.03%
DnCNN-GRU	8.13%	3.88%	3.46%
SFsRNet	**7.32%**	**2.28%**	**0.96%**

Figure 10 presents a comparison of the detection errors of component frequencies for the above six methods under different numbers of components. Among them, figures (a) to (d) respectively represent the detection errors of frequencies when the number of component signals m in the mixed signal is 2 to 5. As can be seen from the figure, the detection error values of the SFsRNet method under different numbers of component signals are all lower than those of the other five methods.

When $SNR \geq 0$ dB, Table 8 presents the average frequency detection errors of the above six methods under different numbers of components. When $m = 4$ and $m = 5$, the average frequency detection errors of the SFsRNet method are 3.57% and 3.47%, respectively, which are 1.88% to 10.93% and 2.55% to 24.09% lower than those of the other methods. This shows that under this condition, the SFsRNet method is less influenced by the number of component signals in the mixed signal. As the number of component signals increases, the advantage of the SFsRNet method in frequency detection performance becomes more and more obvious.

Figures 11 and 12 respectively present the frequency detection accuracy rates of the above six methods under the conditions of frequency error thresholds $\varepsilon = 0.02$ and $\varepsilon = 0.01$. It can be directly observed that under different error threshold values, the detection accuracy rate of the SFsRNet method is superior to that of the other five methods.

Table 9 presents the average frequency detection accuracy rates of the above six methods under the condition of $SNR \geq 0$ dB. For $\varepsilon = 0.01$, the average frequency detection accuracy rate of SFsRNet is 90.66%, which is 9.51% to 38.27% higher than that of the other five methods. For $\varepsilon = 0.02$, the average frequency detection accuracy rate of SFsRNet is 94.48%, which is 2.18% to 24.23% higher than that of the other methods. Thus, it can be

observed that the SFsRNet method still exhibits a good frequency detection effect even under a lower error threshold value, and its advantage becomes more prominent.

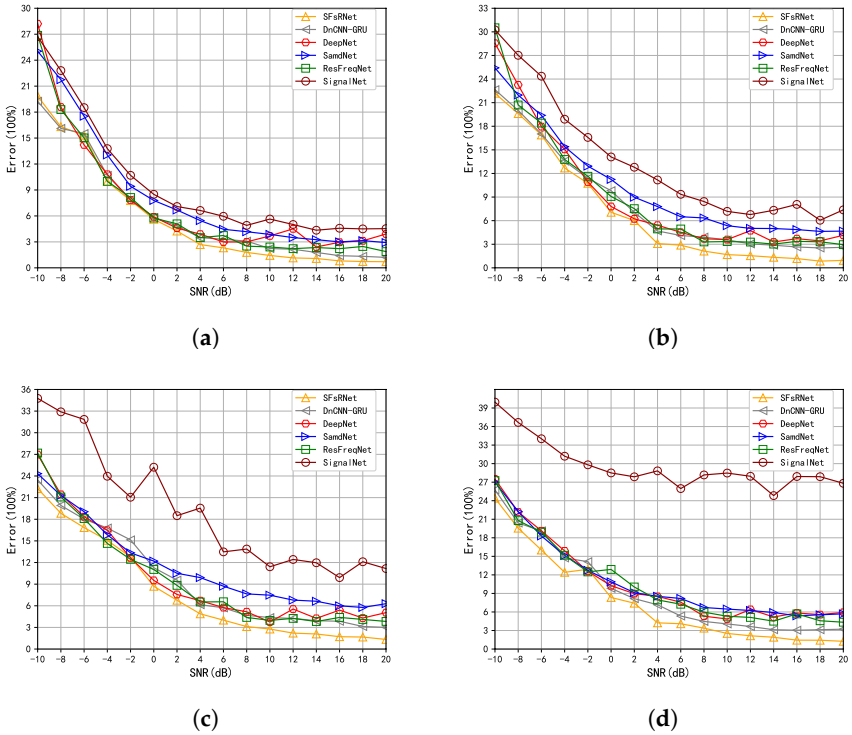

Figure 10. Comparison of frequency detection error with different number of components. (**a**) Frequency detection error value when $m = 2$. (**b**) Frequency detection error value when $m = 3$. (**c**) Frequency detection error value when $m = 3$. (**d**) Frequency detection error value when $m = 3$.

Table 8. Frequency detection error with different number of components.

Method Name	$m = 2$	$m = 3$	$m = 4$	$m = 5$
DeepNet	3.72%	4.59%	5.72%	6.76%
ResFreqNet	3.1%	4.45%	5.6%	6.69%
SignalNet	5.6%	8.96%	14.5%	27.56%
SamdNet	4.38%	6.4%	7.99%	8.91%
DnCNN-GRU	2.79%	4.25%	5.45%	6.02%
SFsRNet	**2.05%**	**2.61%**	**3.57%**	**3.47%**

Table 9. Component frequency detection accuracy under different error thresholds.

Method Name	$\varepsilon = 0.01$	$\varepsilon = 0.02$
DeepNet	74.43%	88.53%
ResFreqNet	76.44%	90.09%
SignalNet	52.39%	70.25%
SamdNet	64.74%	85.56%
DnCNN-GRU	81.15%	92.37%
SFsRNet	**90.66%**	**94.48%**

Figure 13 presents a comparison of the detection accuracy rates of component frequencies for the above six methods under different numbers of components. Among them, figures (a) to (d) respectively represent the detection accuracy rates of frequencies when the number of components in the mixed signal is 2 to 5. As can be seen from the figure, the detection accuracy rate of the SFsRNet method under different numbers of components is superior to that of other methods.

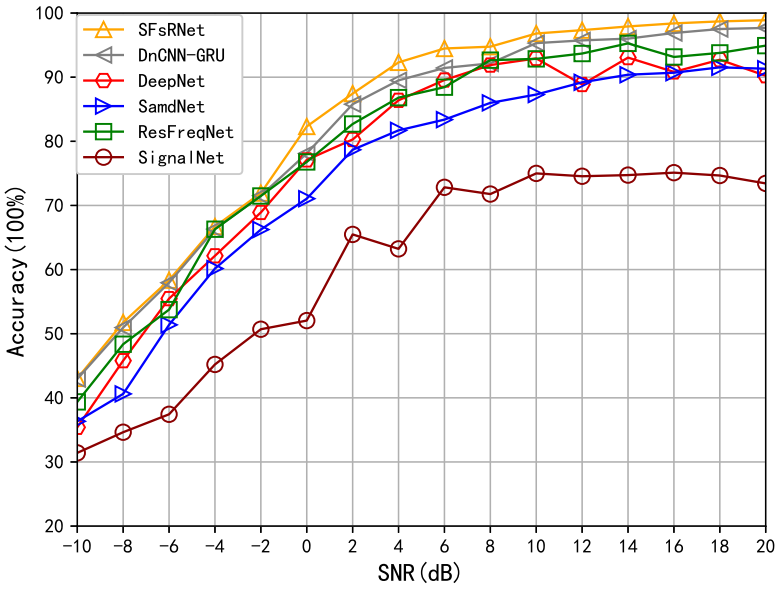

Figure 11. Comparison of component frequency detection accuracy ($\varepsilon = 0.02$).

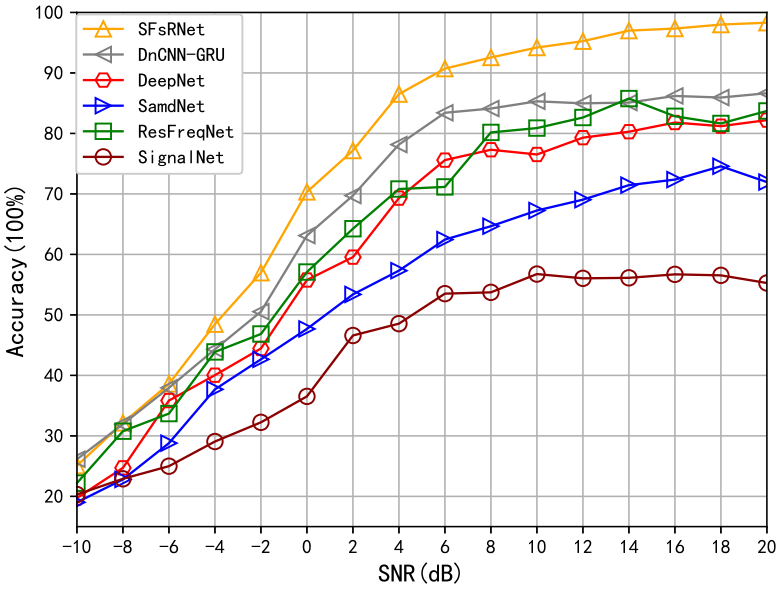

Figure 12. Comparison of component frequency detection accuracy ($\varepsilon = 0.01$).

Table 10 presents the average frequency detection accuracy rates of the above six methods under different numbers of components when $SNR \geq 0$ dB. The average frequency detection accuracy rates of SFsRNet under different numbers of components are 96.43%, 92.88%, 87.9%, and 87.61%, respectively, which are 2% to 29.91%, 9.62% to 43.66%, 7.02% to 45.79%, and 13.15% to 50.56% higher than those of the other five methods. From this, it is evident that SFsRNet boasts a relatively high detection accuracy rate under diverse numbers of components. Furthermore, as the quantity of components grows, the superiority of this method becomes increasingly prominent.

Table 11 presents a comparison of the complexity of six methods, including SFsRNet, under the same experimental environment. Evaluated from the perspectives of the number of parameters and computational complexity, the complexity of SFsRNet is higher than that of ResFreqNet and SignalNet but lower than that of DeepNet and SamdNet. From the perspective of inference time evaluation, the inference time of SFsRNet is comparable to

that of ResFreqNet and significantly better than that of the other five networks. It can thus be seen that SFsRNet is an efficient frequency detection network.

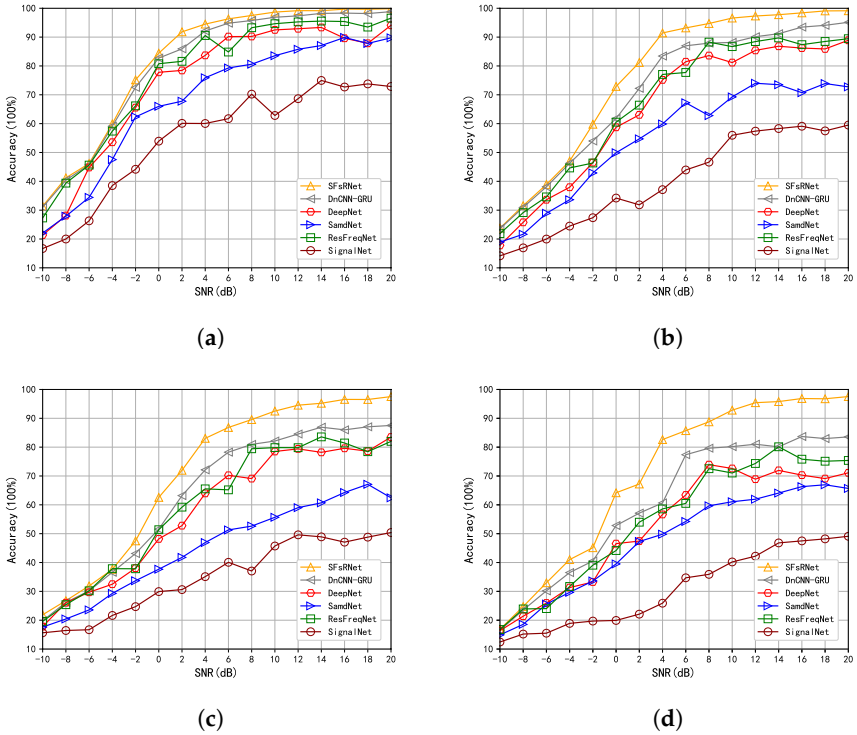

Figure 13. Comparison of frequency detection accuracy with different number of components ($\varepsilon = 0.02$). (**a**) Frequency detection accuracy value when m = 2. (**b**) Frequency detection accuracy value when m = 3. (**c**) Frequency detection accuracy value when m = 3. (**d**) Frequency detection accuracy value when m = 3.

Table 10. Frequency detection accuracy with different number of components.

Method Name	$m = 2$	$m = 3$	$m = 4$	$m = 5$
DeepNet	88.23%	79.67%	71.09%	64.72%
ResFreqNet	91.08%	81.83%	73.25%	67.41%
SignalNet	66.52%	49.22%	42.11%	37.05%
SamdNet	81.21%	66.24%	54.5%	55.86%
DnCNN-GRU	94.43%	85.86%	78.28%	74.46%
SFsRNet	**96.43%**	**92.88%**	**87.9%**	**87.61%**

Table 11. Comparative complexity analysis.

Method Name	Parameters (M)	Computational Complexity (M)	Training Time (ms)	Inference Time (ms)
DeepNet	15.8	74.87	611	2.48
ResFreqNet	13.04	32.89	278	1.72
SignalNet	6.5	50.41	472	2.13
SamdNet	4.85	65.26	491	2.19
DnCNN-GRU	14.69	71.44	531	2.33
SFsRNet	4.9	56.92	364	1.86

5. Conclusions

In this paper, a mixed-signal frequency detection method for signal reconstruction based on sparse features is proposed. It consists of three parts: signal separation network,

component number detection network, and component frequency detection network. By extracting the sparse features of each component signal in the mixed signal, the method constructs the nonlinear reconstruction function of the signal to achieve the separation of each component signal. Based on this, the detection of component number and frequency is realized. Through the verification and analysis of the signal separation ability, number of components, and frequency detection performance of the SFsRNet method, it is proved that this method can effectively separate signals, reduce the mutual interference between component signals and noises, enhance the detection accuracy of the number of components and frequency under low frequency resolution conditions, and enhance the perception of the UAV communication system regarding the electromagnetic environment, thereby further increasing the efficiency of data transmission by UAV.

Author Contributions: Conceptualization, Y.W. and Y.F.; Methodology, Y.W.; Validation,Y.F. and F.Z.; Writing—original draft preparation, Y.W.; Writing—review and editing, Y.F., F.Z., X.C., J.W. and P.Z. All authors have read and agreed to the published version of the manuscript.

Funding: This work was partially supported by National Natural Science Foundation of China (Grant No. 61971291, No. 62471493), Xingliao Talents Plan (Grant No. XLYC2202013), Shenyang Science and Technology Program (Grant No. 23-503-6-16), Shandong Provincial Natural Science Foundation (Grant No. ZR2023LZH017, No. ZR2024MF066), Joint Fund of the Ministry of Education for Pre-Equipment Research 2023, ShenyangYouth Science and Technology Innovation Talent Sup-port Program (Grant No. RC220458) and Central Guidance Local Special Project in 2024.

Institutional Review Board Statement: Not applicable.

Informed Consent Statement: Not applicable.

Data Availability Statement: The data that support the findings of this study are available from the corresponding author upon reasonable request.

Conflicts of Interest: The authors declare no conflicts of interest.

Abbreviations

The following abbreviations are used in this manuscript:

UAV	Unmanned Aerial Vehicle
SNR	Signal-to-Noise Ratio
SFsRNet	Sparse Feature Signal Reconstruction Network Framework
MSE	Mean Square Error
Conv	Convolutional Layer
Pool	Max Pooling Layer
ReLU	Rectified Linear Unit
FC	Fully Connected Layer
TConv	Transposed Convolution Layer
BN	Batch Normalization Layer
SGE	Spatial Group-wise Enhance
Adam	Adaptive Moment estimation

References

1. Huang, Y.; Cui, H.; Hou, Y.; Hao, C.; Wang, W.; Zhu, Q.; Li, J.; Wu, Q.; Wang, J. Space-based Electromagnetic Spectrum Sensing and Situation Awareness. *Space Sci. Technol.* **2024**, *4*, 0109. [CrossRef]
2. Zhou, B.; Ma, X.; Kuang, T.; Li, J. New Paradigm of Electromagnetic Spectrum Space Situation Cognition: Spectrum Semantic and Spectrum Behavior. *Data Acquis. Process.* **2022**, *37*, 1198–1207.
3. Wang, Y.; Zou, N.; Fu, J.; Liang, G.L. Transient Signal Detection Method Based on Partial Instantaneous Energy Density Level. *Electron. Inf. Technol.* **2013**, *35*, 1720–1724. [CrossRef]

4. Josip, L.; Ivana, R.; Dinko, B. A Survey on the Energy Detection of OFDM Signals with Dynamic Threshold Adaptation: Open Issues and Future Challenges. *Sensors* **2021**, *21*, 3080. [CrossRef]
5. Vartiainen, J.; Karvonen, H.; Matinmikko-Blue, M.; Mendes, L.; Saarnisaari, H.; Matos, A. Energy Detection Based Spectrum Sensing for Rural Area Networks. *EAI Endorsed Trans. Wirel. Spectr.* **2020**, *4*, e6. [CrossRef]
6. Wu, W.; Wang, Z.; Yuan, L.; Zhou, F.; Lang, F.; Wang, B.; Wu, Q. IRS-enhanced energy detection for spectrum sensing in cognitive radio networks. *IEEE Wirel. Commun. Lett.* **2021**, *10*, 2254–2258. [CrossRef]
7. Yoo, S.K.; Sofotasios, P.C.; Cotton, S.L.; Muhaidat, S.; Badarneh, O.S.; Karagiannidis, G.K. Entropy and Energy Detection-Based Spectrum Sensing Over F-Composite Fading Channels. *IEEE Trans. Commun.* **2019**, *67*, 4641–4653. [CrossRef]
8. Dibal, P.Y.; Onwuka, E.N.; Agajo, J.; Alenoghena, C.O. Wideband spectrum sensing in cognitive radio using discrete wavelet packet transform and principal component analysis. *Phys. Commun.* **2020**, *38*, 100918. [CrossRef]
9. El Khamy, S.E.; Abd el Malek, M.B.; Kamel, S.H. A stationary wavelet transform approach to compressed spectrum sensing in cognitive radio. *Int. J. Commun. Syst.* **2017**, *30*, e3140. [CrossRef]
10. Kumar, A.; Saha, S.; Bhattacharya, R. Wavelet transform based novel edge detection algorithms for wideband spectrum sensing in CRNs. *AEU—Int. J. Electron. Commun.* **2018**, *84*, 100–110. [CrossRef]
11. Mukherjee, N.; Chattopadhyaya, A.; Chattopadhyay, S.; Sengupta, S. Discrete-wavelet-transform and stockwell-transform-based statistical parameters estimation for fault analysis in grid-connected wind power system. *IEEE Syst. J.* **2020**, *14*, 4320–4328. [CrossRef]
12. Zhou, F.; Xu, W.; Yuan, J.; Tian, B.; Li, J. Research on the Joint Optimization of Hop Period Estimation Method for Link16 Signals. *J. Shenyang Ligong Univ.* **2022**, *41*, 14–19.
13. Osadchiy, A.; Kamenev, A.; Saharov, V.; Chernyi, S. Signal processing algorithm based on discrete wavelet transform. *Designs* **2021**, *5*, 41. [CrossRef]
14. Zhou, R.; Zhang, Y.; Sun, X.; Guo, C. A cooperative spectrum sensing algorithm based on Bayesian compressed sensing. In Proceedings of the 2017 3rd IEEE International Conference on Computer and Communications (ICCC), Chengdu, China, 13–16 December 2017; pp. 658–662.
15. Yan, S. Collaborative spectrum sensing for cognitive radio networks by using 1-bit compressed sensing. In Proceedings of the 4th International Conference on Communication and Information Processing, Qingdao, China, 2–4 November 2018; pp. 289–293.
16. Zhao, J.; Liu, Q.; Wang, X.; Mao, S. Scheduled sequential compressed spectrum sensing for wideband cognitive radios. *IEEE Trans. Mob. Comput.* **2017**, *17*, 913–926. [CrossRef]
17. Zhang, X.; Tan, H.; Lyu, W. Low-complexity generalized space shift keying signal detection algorithm based on compressed sensing. *Comput. Appl.* **2023**, *43*, 3890–3895.
18. Li, S.; Shang, J.; Chen, Q.; Sun, Y.; Liu, J.X. A compressed sensing based two-stage method for detecting epistatic interactions. *Int. J. Data Min. Bioinform.* **2016**, *14*, 354–372. [CrossRef]
19. Zhang, H.; Dong, Z.; Sun, M.; Gu, H.; Wang, Z. TP-CNN: A Detection Method for atrial fibrillation based on transposed projection signals with compressed sensed ECG. *Comput. Methods Programs Biomed.* **2021**, *210*, 106358. [CrossRef]
20. Feng, J.; Yang, L.T.; Ren, B.; Zou, D.; Dong, M.; Zhang, S. Tensor Recurrent Neural Network With Differential Privacy. *IEEE Trans. Comput.* **2024**, *73*, 683–693. [CrossRef]
21. Borylo, P.; Biernacka, E.; Domzal, J.; Kadziolka, B.; Kantor, M.; Rusek, K.; Skala, M.; Wajda, K.; Wojcik, R.; Zabek, W. Neural Networks in Selected Aspects of Communications and Networking. *IEEE Access* **2024**, *12*, 132856–132890. [CrossRef]
22. Ding, X.; Ni, T.; Zou, Y.; Zhang, G. Deep learning for satellites based spectrum sensing systems: A low computational complexity perspective. *IEEE Trans. Veh. Technol.* **2022**, *72*, 1366–1371. [CrossRef]
23. Pan, X.; Cao, K. Spectrum Sensing Based on CNN-LSTM with Attention for Cognitive Radio Networks. In Proceedings of the 2023 8th International Conference on Intelligent Informatics and Biomedical Sciences (ICIIBMS), Okinawa, Japan, 23–25 November 2023; Volume 8, pp. 63–67.
24. Mehrabian, A.; Sabbaghian, M.; Yanikomeroglu, H. CNN-based detector for spectrum sensing with general noise models. *IEEE Trans. Wirel. Commun.* **2022**, *22*, 1235–1249. [CrossRef]
25. Wang, Y.; Feng, Y.X.; Song, B.X.; Qian, B. Spectrum sensing method for wireless signals based on kurtosis estimation. *Acta Armamentarii* **2024**, 1–12. [CrossRef]
26. Izacard, G.; Bernstein, B.; Fernandez Granda, C. A learning-based framework for line-spectra super-resolution. In Proceedings of the ICASSP 2019-2019 IEEE International Conference on Acoustics, Speech and Signal Processing (ICASSP), Brighton, UK, 12–17 May 2019; pp. 3632–3636.
27. Izacard, G.; Mohan, S.; Fernandez Granda, C. Data-driven estimation of sinusoid frequencies. In *Advances in Neural Information Processing Systems*; Cornell University Library: Ithaca, NY, USA, 2019; pp. 5127–5137.
28. Pan, P.; Zhang, Y.; Deng, Z.; Qi, W. Deep learning-based 2-D frequency estimation of multiple sinusoidals. *IEEE Trans. Neural Netw. Learn. Syst.* **2021**, *33*, 5429–5440. [CrossRef] [PubMed]

29. Dreifuerst, R.M.; Heath, R.W. Signalnet: A low resolution sinusoid decomposition and estimation network. *IEEE Trans. Signal Process.* **2022**, *70*, 4454–4467. [CrossRef]
30. Guo, Y.; Bao, Y.; Li, H.; Zhang, Y. Deep learning-based adaptive mode decomposition and instantaneous frequency estimation for vibration signal. *Mech. Syst. Signal Process.* **2023**, *199*, 110463. [CrossRef]
31. Yang, H.; Monte-Moreno, E.; Hernández-Pajares, M.; Roma-Dollase, D. Real-time interpolation of global ionospheric maps by means of sparse representation. *J. Geod.* **2021**, *95*, 71. [CrossRef]
32. Zha, Z.; Yuan, X.; Wen, B.; Zhang, J.; Zhou, J.; Zhu, C. Image restoration using joint patch-group-based sparse representation. *IEEE Trans. Image Process.* **2020**, *29*, 7735–7750. [CrossRef]
33. Feng, J.; Yang, L.T.; Zhu, Q.; Choo, K.K.R. Privacy-Preserving Tensor Decomposition Over Encrypted Data in a Federated Cloud Environment. *IEEE Trans. Dependable Secur. Comput.* **2020**, *17*, 857–868. [CrossRef]
34. Wang, X.; Zhang, K.; Wang, J.; Jin, Y. An Enhanced Competitive Swarm Optimizer With Strongly Convex Sparse Operator for Large-Scale Multiobjective Optimization. *IEEE Trans. Evol. Comput.* **2022**, *26*, 859–871. [CrossRef]
35. Yang, J.; Wright, J.; Huang, T.; Ma, Y. Image Super-Resolution Via Sparse Representation. *IEEE Trans. Image Process.* **2010**, *19*, 2861–2873. [CrossRef]
36. Li, X.; Hu, X.; Yang, J. Spatial Group-wise Enhance: Improving Semantic Feature Learning in Convolutional Networks. arXiv, 2019, arXiv:1905.09646.
37. Giang, T.L.; Dang, K.B.; Le, Q.T.; Nguyen, V.G.; Tong, S.S.; Pham, V.M. U-Net convolutional networks for mining land cover classification based on high-resolution UAV imagery. *IEEE Access* **2020**, *8*, 186257–186273. [CrossRef]
38. Li, G.; Gu, X.; Chen, C.; Zhou, C.; Xiao, D.; Wan, W.; Cai, H. Low-Frequency Magnetotelluric Data Denoising Using Improved Denoising Convolutional Neural Network and Gated Recurrent Unit. *IEEE Trans. Geosci. Remote Sens.* **2024**, *62*, 5909216. [CrossRef]